

# Mathematical Modeling Technique

R. T. Longo\*  
rtlongo370@gmail.com

Copyright ©2018 Dr. Robert T. Longo, All Rights Reserved

March 14, 2018

## Abstract

In this paper, a general modeling principle is introduced that was found useful for modeling complex physical systems for engineering applications. The technique is a nonlinear asymptotic method (NLAM), constructed from simplified physical theories, i.e., physical theories that were developed from particular points of view, that can be used to construct a more global theory. Originally, the technique was envisioned primarily for engineering applications, but its success has led to a more general principle. Four examples are presented to discuss and illustrate this method.

## 1 INTRODUCTION

Often, practical engineering requires knowledge of how physical processes change with time or in regions of interest between physical theories that do not overlap. The physical laws that govern the beginning of a process often are different from the laws that govern at the end of the process, and, often, there is no complete physical law that connects the two. In such cases, investigators often resort to generating empirical formulas. This type of data fitting usually works well in certain regions of interest, but it fails completely when extended and does not preserve the underlying physics. In this paper, we discuss a modeling technique that fits well in all regions of interest not covered by the basic theories and that also preserves the physical laws underlying the processes.

The first application of this technique was used while developing a life model for dispenser cathodes, Longo [1, 2, 3]. The dispenser cathode degrades slowly, and its emission transitions between two well-known physical laws, i.e., the Richardson [4], Dushman [5], Schottky [6] law and the Child [7], Langumire [8] law. There is no complete physical law that connects these two laws. The life expectancy of cathodes is very important in the application of communication satellites and in deep space missions, both of which depend on the satellites

---

\*Physicist and Technical Fellow, Boeing Aircraft Company, retired

having long lives and stable outputs. This technique has proved to be useful for extending the life of Dispenser cathodes that have high current densities.<sup>1</sup> Over time it was shown that this modeling technique, a relatively simple emission formula, was an accurate description of the physical processes even though it was not derived from fundamental physics. Recently, it has been observed that the strategy used to obtain the emission equation can be applied to numerous other physical problems. The purpose of this paper is to introduce a strategy that can be described as a general principle referred to as the nonlinear asymptotic method (NLAM). The principle is illustrated by four examples from different physics disciplines.

Sometimes, empirical rules are used for such a long time and have such an impact on basic physics that they become an integral part of the underlying theory. One good example of this is the Matthiessen [9] rule, which is an empirical relationship (based on experimental observations) that describes the resistivity of very dilute alloy metals. Basically, it states that the resistivity of metals is composed of the sum of two parts, i.e., the resistivity of the pure metal due to crystal lattice vibrations and the resistivity of a non-pure part due to strains, defects, and impurities. The sum is just a linear combination of these two parts. Over the years, this rule has been used to study metals, and it has been used extensively in the development of solid state materials. The inherently unsatisfactory nature of this empirical sum rule has generated many theoretical papers aimed at calculating the resistivity of dilute alloy metals from basic principles in an effort to test Matthiessen's rule. In general, these efforts are referred to as the "Deviation from Matthiessen's Rule" (DMR). An excellent review was given by Bass [10]. Basically, Matthiessen's rule is the linear sum of two perceived distinct parts.

$$\rho = \rho_T + \rho_I \tag{1}$$

where  $\rho_T$  is the resistivity of the pure metal (phonon scattering), and  $\rho_I$  is the impurity part (fixed impurity-electron scattering). In terms of conductivity, this can be written as:

$$\frac{1}{\sigma} = \frac{1}{\sigma_T} + \frac{1}{\sigma_I} \tag{2}$$

When there is a need to calculate electron scattering or relaxation times in which two discrete processes are involved, it is usually taken to be:

$$\frac{1}{\tau} = \frac{1}{\tau_0} + \frac{1}{\tau_I} \tag{3}$$

Similarly, combining discrete processes leads to a similar formula for mobility:

---

<sup>1</sup>NASA's Deep space Cassini mission, for example, would be limited without TWTs with both high power and long life.

$$\frac{1}{\mu} = \frac{1}{\mu_0} + \frac{1}{\mu_I} \quad (4)$$

In fact, the reduced mass used in the quantum theory of the hydrogen atom has been found to follow a rule that is functionally similar:

$$\frac{1}{m} = \frac{1}{m_{proton}} + \frac{1}{m_{electron}} \quad (5)$$

The form of these equations have been used in many theoretical works, sometimes without justification, Shockley [11]. In effect, all of these equations are linear combinations of variables, constants, or distinct physical processes.

In this paper, the linear combination of asymptotic processes is generalized into a more general, nonlinear combination. A generalized technique for modeling physical processes is introduced in which the Matthiessen rule is just one special case. This nonlinear asymptotic modeling technique is illustrated by four specific examples from very different physical fields of study. The first example is from thermionic emission, the process that led to this work. The second example is the determination of the drag coefficient through the transition from laminar to turbulent flow. The third example is a re-visit of Matthiessen's rule and a demonstration that the nonlinear asymptotic formulation offers an explanation for all of the fine, detailed features observed by studies of DMR. The fourth example uses the nonlinear asymptotic technique to construct a complex theory of surface physics by developing two simple asymptotic physical theories and then forming the final result as a nonlinear combination.

## 2 BACKGROUND

The empirical rule discussed here first was used to describe thermionic emissions as applied to traveling wave tubes (TWTs) (Gilmour, [12]). It was observed that the well known theories of thermionic emissions worked very well only at the extremes, well outside of the practical range of operation. The well-known theory of space charge emission, as first solved by Child [7] and later by Langmuir [8], do not fit well with results observed as the accelerating voltage is increased or the temperature of the emitter is decreased. Furthermore, the thermodynamic solution developed by Richardson [4], Dushman [5], and Schottky [6] is in all practical application of TWTs completely outside the normal TWT operating range. For TWTs, all measurements are made in a region that is somewhere between the two well-known extremes. With the Richardson-Dushman-Schottky limit, it is impossible to reach this region under normal operating conditions because of restrictions placed on the measurements of TWT's so as to prevent damage. However, pulsed measurements can be used even though they generally are not acceptable because they are not representative of actual operation. In order to proceed with the problem, an empirical formula was developed that

worked reasonably well, but, as was the case with the Matthiessen rule, it was not perfectly accurate. This empirical formula was obtained by taking the solutions to the two well known theories and forming a linear combination as a reciprocal sum Longo [ 1, 2, 3].

$$\frac{1}{J} = \frac{1}{J_{sc}} + \frac{1}{J_{tl}}. \quad (6)$$

Equation 6 is similar in form to Equations 1 , 2, 3, 4, and 5, and it provides a measure of the current density, J, in terms of two asymptotic emission theories, the space charge limit,  $J_{sc}$ , the solution to the space charge theory, i.e., the Child or Langmiur theory, and  $J_{tl}$ , the solution to the temperature-limited thermionic theory, i.e., the Richardson-Dushman-Schottky theory. It is easy to show that Equation 6 approaches the space charge theory and the temperature-limited theory correctly in all limits. Although the linear combination, i.e., Equation 6, has the proper behavior, in general, it has a smaller curvature in the transition region (i.e., it has a more rounded curve) than observed, and the curvature cannot be controlled by the internal parameters of either  $J_{tl}$  or  $J_{sc}$ . In order to get a better representation of the observed data, an adjustable, unit-less parameter is used that will directly affect the curvature Vaughan [13].

$$\frac{1}{J^\alpha} = \frac{1}{J_{sc}^\alpha} + \frac{1}{J_{tl}^\alpha}. \quad (7)$$

This modification provides a virtually perfect representation of the observed data, at least within the accuracy of the measurements. Clearly,  $\alpha$  has the maximum effect at the transition between  $J_{tl}$  and  $J_{sc}$ , and its effect is eliminated as each asymptotic limit is approached.

## 2.1 The generalization of the nonlinear asymptotic technique

It should be observed that the general practice of forming combinations of distinct physical processes, as is done in Equations 1, 2, 3, 4, and 5, only mixes those processes linearly. By including an adjustable parameter, as in Equation 7, the physical processes are mixed in a nonlinear way. One way to obtain more insight into the nature of Equation 7 is to write it in the form:

$$J^\gamma = J_{sc}^\gamma + J_{tl}^\gamma. \quad (8)$$

where  $\alpha$  is replaced by  $-\gamma$ . This gives a functional form that is suggestive of a geometric vector length, S, in Euclidian space, i.e.,  $S^2 = x^2 + y^2$ , with  $\gamma = 2$ , that also mixes the geometric space coordinates of a particular coordinate system in a nonlinear way to arrive at a measure (a metric) of the length of a vector. We will use this similarity to the space metric as guidance for obtaining further insight concerning the properties of nonlinear asymptotic mixing (NLAM), i.e., Equation 7. The quantity, J, in Equation 8 is a measure of a physical property described by the generating function  $\{J_{sc}, J_{tl}\}$ , as is the vector length S, which

is described by the coordinates  $\{x, y\}$ . The generalized quantity does not have to be a geometric object; rather, it can describe any physical property as long as all of the parts have the same units or have multiplying factors that bring them to the same units.

There are interesting similarities with the Euclidean space metric that will be useful in the generalization. In ordinary Euclidean space, the length of the geometric vector has the form  $S^2 = x^2 + y^2$ , and the generating functions,  $\{x, y\}$ , are independent. The meaning of the independence of  $\{x, y\}$  is understood easily in terms of the orthogonality of space. This property of component independence can be carried over to the generalization. The meaning of independence is not as obvious in the general case as it is in the geometric case, however, it will be shown that the generating functions  $\{J_{sc}, J_{tl}\}$  for emissions, Equation 8, are independent variables. The independence of  $\{J_{sc}, J_{tl}\}$  will be discussed in more detail in Example 1 in Section 3, below.

By pursuing this direction, certain properties of the Euclidian space can provide guidance for the general case, such as invariance under certain transformations, e.g., rotational invariance. Rotational transformation mixes the generating functions but leaves the metric (i.e., the vector length in geometric applications ) invariant. As shown below, the generalized metric, which we will call the NLAM-metric, can be made rotational invariant if the independent generating functions, e.g.,  $X$ , are taken to be  $X^{\gamma/2}$ . This is shown in Appendix A. This means that any linear transformations of  $X$ s will be made by using  $X^{\gamma/2}$ . Example 3 shows that this feature has a meaningful contribution by showing that it enhances the result.

The parameter  $\gamma$  in equation 8 can take any real value, positive or negative, depending on the application. If a parameter,  $m$ , is defined as,  $m = 1/\gamma$ , a physical interpretation can be given to  $m$ . The parameter,  $m$ , can be thought of as a measure of the mixing of the independent variables. If there is no mixing at all,  $m$  is small, and there is very little mixing; the result follows one variable until it becomes equal in magnitude to the other, thereafter the result follows the second variable, and the metric will have a sharp transition between the two generating functions. In the case of a length in Euclidean space,  $m = 1/2$  can be interpreted as equal mixing or equal weights of the two space dimensions in the final length result. The mixing parameter does not depend on the dimensionality of space since the total metric can be built by repeated applications of a 2-D space, e.g., in Euclidean space,  $S^2 = U^2 + z^2$ , where  $U^2 = x^2 + y^2$ . In the case of the nonlinear, asymptotic technique, there would be more than two generating theories, as demonstrated in example 2 in section 4, below.

Five principles that can be used when generating a theoretical model using the nonlinear asymptotic modeling technique are described below.

*Principle I*

From independent points of view, a physical problem that can be composed of two or more distinct and independent theories describing a common property can be formed into a more complete theory by the application of the nonlinear asymptotic modeling technique.

*Principle II*

All generating theories must be complete over the entire range of the independent internal physical variables. The data must go all the way to the asymptote. The functions that are used cannot be truncated expansions of more complete theories.

*Principle III*

The generating theories must be independent developments of the same physical properties, i.e., they must have the same units or factors that cause them to have the same units. The independence is determined from the set of assumptions used in their development.

*Principle IV*

Linear transformations can be used to test the independence of the generating theories, and they can be used to correct for non-independence.

*Principle V*

The inability of the metric to adequately provide a measure of a physical process suggests that components or theories are missing.

The remainder of this paper applies these principles to four specific examples and attempts to clarify the general concept.

### **3 EXAMPLE 1: THERMIONIC EMISSION**

Some of the aspects of modeling thermionic emission have been discussed in the preceding section. In this example, the meaning of the independence of  $\{J_{sc}, J_{tl}\}$  is examined, and the fidelity to which this modeling technique describes real experimental data is demonstrated.

#### **3.1 Independence of $\{J_{sc}, J_{tl}\}$**

The sense of independence of the generating functions,  $J_{sc}$  and  $J_{tl}$ , can be understood as follows: The space charge current density,  $J_{sc}$ , is derived from a theory that has a set of assumptions that is completely different and independent from the set of assumptions used to derive the temperature-limited current

density,  $J_{tl}$ . In this sense, these two theories are independent views that describe the same physical property, i.e., current flow. The sets of assumptions for space charge emission are shown in Table1.

Table 1: Assumption for  $J_{sc}$  theory

Vacuum space charge	$\rho_s$
Electrostatic process	$\nabla^2\phi = \rho_s$
Anode to cathode spacing	$d$
Geometry of the vacuum vehicle	$K = \frac{2.66 \times 10^{-6}}{d^2}$
Potential that returns excess electron to cathode	$\phi_{min}$

The assumptions in Table1 lead to a current density,  $J_{sc}$ , that first was derived by Child [7].

$$J_{sc} = KV^{3/2}. \quad (9)$$

This current density depends on the applied voltage,  $V$ , and the geometry,  $K$ , of the vacuum vehicle in which the emitter is enclosed. It is independent of the properties of the thermionic emitter, including its temperature. As can be seen from the assumption in Table 1, the space charge theory assumes nothing about the emitter other than that it emits as much current as needed, focusing only on the charge that fills the geometric volume of the vacuum device that encloses the emitter and the applied electric field. The set of assumptions for temperature-limited emission,  $J_{tl}$ , is shown in Table 2.

Table 2: Assumption for  $J_{tl}$  theory

Thermodynamics controls available electrons	$\rho_M e^{-\frac{e\phi}{k_B T}}$
Cathode material controls work function	$\phi$
Results are independent of geometry	
All emitted electrons are assumed to be removed from problem	

The assumptions in Table 2 lead to the current density,  $J_{tl}$  Richardson [4], Dushman [5]

$$J_{tl} = AT^2 e^{-e\phi/kT} f_s(V, T). \quad (10)$$

Where the Schottky function, Schottky [6],  $f_s(V, T)$ , is given by

$$f_s(V, T) = e^{\beta\sqrt{V/T}}, \quad (11)$$

where  $A = \frac{4\pi m e k^2}{\hbar^3}$ , and  $\beta = \frac{e}{k} \sqrt{\frac{e}{4\pi\epsilon_0 d}}$ .

The temperature limited current density,  $J_{tl}$ , is derived from a theory that focuses on the thermodynamics of the emitter and assumes nothing about the geometry of the enclosing device or the field in the device, except that the fields are so high that all electrons emitted from the surface are permanently removed, after which they have no further influence on the physics of the problem.

This example illustrates the concept of the independence of the generating functions. Each asymptotic theory describes the physical process of electron current flow from a totally different perspective with no overlap (perhaps with the exception that both assume that electrons are emitted). This example illustrates the application of principles I, II, and III. Note that another important point is that physical measurements usually are made in the intermediate region where neither of the generating functions,  $\{J_{sc}, J_{tl}\}$ , appropriately apply. The result of the NLAM-metric constrains the interpretation of the experimental measurements to an asymptotic trend toward the physical generating functions. This allows practical measurements to extract physical parameters that would otherwise be difficult or impossible to obtain. Furthermore, it is evident that the parameter,  $\gamma$ , has the greatest influence in the transition region but does not affect the asymptotic regions at all, so measurements of the physical parameters of  $J_{sc}$  and  $J_{tl}$  from the transition region are independent of  $\gamma$  and produce accurate results.

Figure 1 shows the experimental data<sup>2</sup> in the J-V plane with temperature as a parameter, overlaid by a fit to Equation 8. The NLAM-metric fit needs only one value of  $\gamma$  for all temperatures.

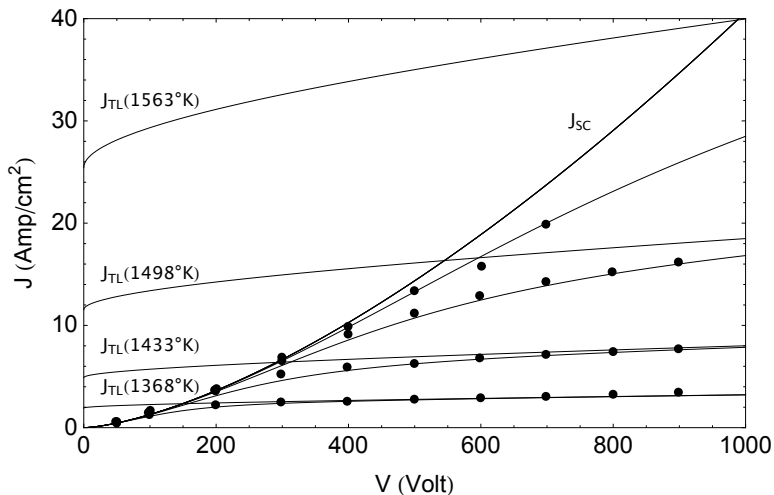


Figure 1: Shows the data fit with equation 7.

<sup>2</sup>These data were taken in a closely-spaced, parallel-plate diode (CSPPD)

In a TWT, voltages are very important for proper operation, so data usually are measured in the J-T plane with voltage as a parameter; even so, the same functions,  $J_{sc}$  and  $J_{tl}$ , still apply. Figure 2 shows the data taken on a TWT, and the measured work function was 1.97 eV, and the  $\gamma$  was 2.2. The model clearly provides an excellent representation of the experimental data in either the J-V or J-T planes.

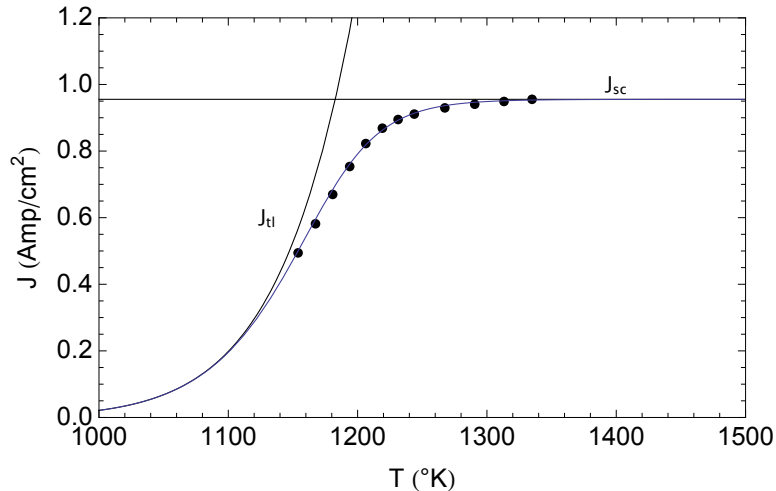


Figure 2: TWT data measured in the J-T plane

## 4 EXAMPLE 2: DRAG COEFFICIENT ON FLUID FLOW THROUGH A SMOOTH PIPE

In this example, the drag coefficient of fluid flow is modeled for the transition from laminar flow to turbulent flow in a smooth pipe. It is clear from the last example that the NLAM-metric always makes a transition at the crossing point of the two generating functions. The resulting curve either lies above the generating functions, with a positive  $\gamma$  or below the generating functions with a negative  $\gamma$ . However, to apply the NLAM-metric, all generating functions must be complete over the entire range of the independent variable (principle II), in this case the Reynolds number, and each must diverge from the others in the unobservable regions so as to contribute only where they are needed. In this example, we used data from American Institute of Physics Handbook [14]. The laminar and turbulent flow generating functions are given by Equations 12 and 13, respectively, and Figure 3 shows them overlying the data.

$$C_L(R) = 10^{4.048 - 1.074 \text{Log}_{10}(R)}. \quad (12)$$

$$C_T(R) = 10^{1.567-0.265\text{Log}_{10}(R)}. \quad (13)$$

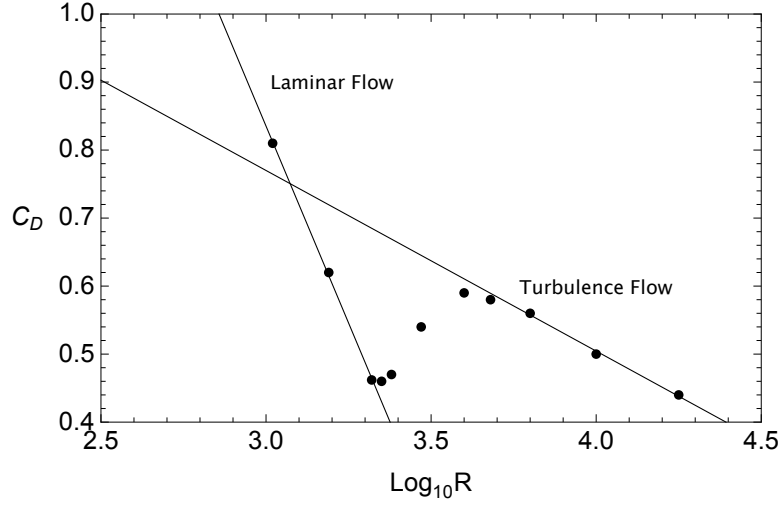


Figure 3: Data and asymptotic functions during the transition from laminar flow to turbulent flow

In this case, Fig. 3 shows that the physical transition from laminar to turbulent flow does not occur at the crossing of the two functions. The NLAM-metric still can be applied by assuming that there is a missing function, i.e., a third generating function that is dominate only near the transition, thus illustrating principle V. It is known that a narrow transition occurs before the onset of turbulent flow. This generating function can be created empirically from the data. Taking the form for the third curve to be the same, the third transition curve is:

$$C_3(R) = 10^{-1.893+0.701\text{Log}_{10}(R)}. \quad (14)$$

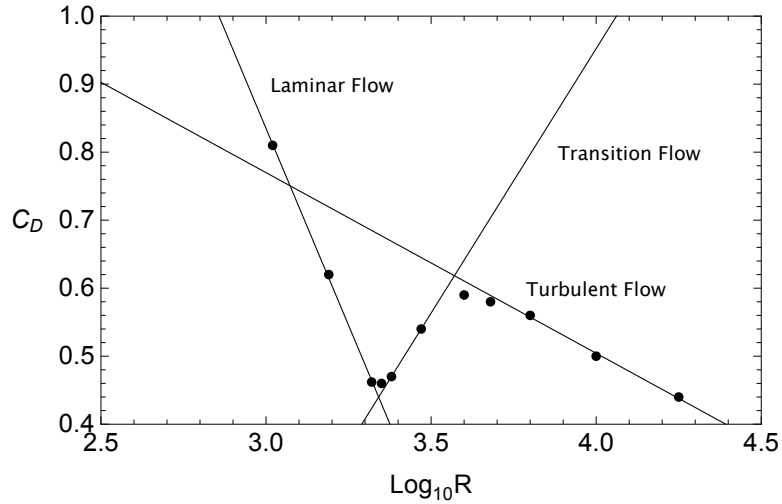


Figure 4: Transition from laminar flow to turbulent flow. The transition flow is not an asymptotic function

The three generating functions shown in Figure 4 clearly capture the dataset. Now, the three components can be modeled into a single curve over the entire range of Reynolds numbers by applying the metric twice. The transition flow is linked to both the turbulent flow and the laminar flow. Furthermore, since the transition flow does not extend all the way to the asymptote in either transition, the two transitions will have to be linked together at a single point, and this point is marked with an "x" in Figure 5. An NLAM-metric must be formed for the transition to turbulent flow and must not be extended beyond the midpoint of the transition region. Similarly, an NLAM-metric must be formed for the laminar-to-transition region, and it is not be extended beyond the chosen point in the transition region; these requirements are reflected in Equations 15 and 16:

$$C_{TURB}(R) = (C_3(R)^\alpha + C_T(R)^\alpha)^{1/\alpha} \quad (15)$$

$$C_{LAM}(R) = (C_3(R)^\beta + C_L(R)^\beta)^{1/\beta} \quad (16)$$

Figure 5 shows the final composite NLAM-metric curve, with  $\alpha = -15$  and  $\beta = 20$ , and it clearly is a respectable representation of the experimental data over the entire range of Reynolds numbers. The final curve, Figure 5, is not a single curve; rather, it consists of two parts, and the point marked with an "x" is where the two parts join. This is necessary because, according to Principle II, each NLAM-metric does not continue all the way to the asymptote.

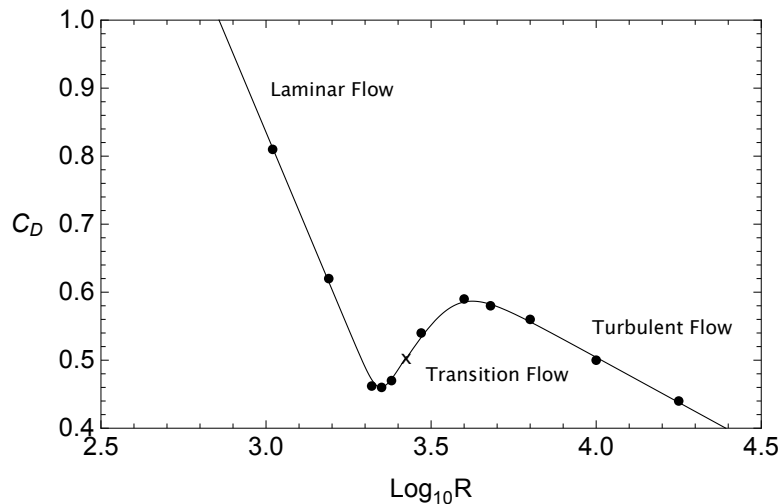


Figure 5: Transition from laminar flow to turbulent flow is linked at the point marked with an x.

## 5 EXAMPLE 3: RESISTIVITY OF DILUTE ALLOY METALS

There has been an extensive theoretical effort to understand and develop a theory for the resistivity of dilute metal alloys that are characterized by Matthiessen's rule. A review of this work, call deviation from Matthiessen's rule (DMR) is given by Bass[10]. These works basically compares the measured resistivity to the resistivity obtained from Matthiessen's rule.

As indicated in the review and references provided by Bardeen [15], the resistivity for pure metals was developed by Bloch-Gruneisen and is given by:

$$\rho_T = \left(\frac{\theta}{T}\right)^{-4} \int_0^{\frac{\theta}{T}} \frac{E^s s^5}{(E^s - 1)^2} ds \quad (17)$$

where  $\theta$  is the Debye temperature characteristic of each metal. From Matthiessen [9], the impurity part can be written as

$$\rho_I = ac + b, \quad (18)$$

where a and b are constants, and c is the atomic percent concentration of impurities. At this point we can make a direct application of the NLAM-metric that gives the total resistivity:

$$\rho = (\rho_T^\gamma + \rho_I^\gamma)^{1/\gamma} \quad (19)$$

This clearly reduces to Mattheissen's rule if  $\gamma = 1$ . To determine if a value for  $\gamma \neq 1$  makes sense, the deviation function measured in most studies of DMR, i.e.,  $\Delta/\rho_I$ , is constructed. The deviation,  $\Delta$ , is defined as the difference between the actual measured resistivity,  $\rho(T, c)$ , and the resistivity given by Mattheissen's rule. Equation 20

$$\Delta = \rho(T, c) - (\rho_T + \rho_I). \quad (20)$$

In this work, we start with the assumption that the resistivity formed by the NLAM-metric is a good representation of the measured resistivity. Thus, we will assume that Equation 19 is a good representation for  $\rho(T, c)$ , so that the deviation function becomes:

$$\frac{\Delta}{\rho_I} = \frac{(\rho_T^\gamma + \rho_I^\gamma)^{1/\gamma}}{\rho_I} - \frac{(\rho_T + \rho_I)}{\rho_I} \quad (21)$$

The general character of the  $\Delta/\rho_I$  curve shown in Figure 6 is correct for most alloy systems, but there are a few characteristics that cannot be generated with Equation 21.

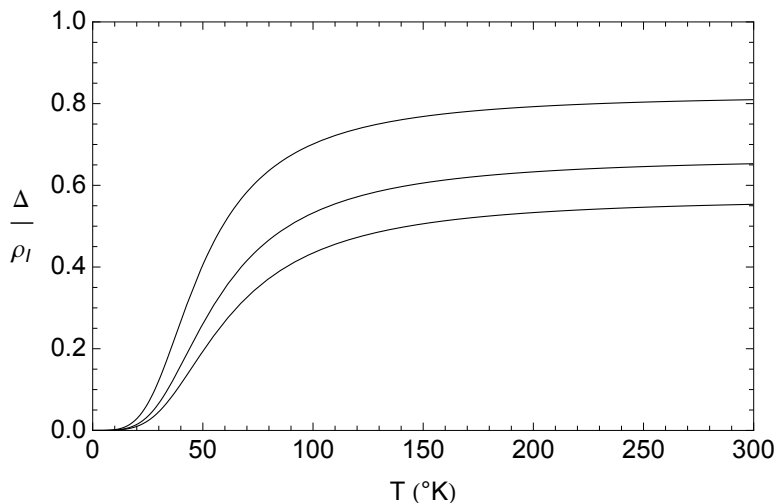


Figure 6: Typical curve for equation 21 vs. temperature.

In many systems, there are features described as a "hard to explain hump" [Bass, [10]]. Our effort is to show that the application of the NLAM-metric can fit the data. It seems that our assumption that the NLAM-metric is a good

representation of the measured resistivity is not valid. To test this, we considered the independence of the two generating functions, i.e., Equations 17 and 18.

In Tables 3 and 4, we examined the assumptions that were made for the two resistivity regions that were used as generating functions. When one examines the general assumptions used to generate these functions, a clear case for independence of these two regions cannot be made from a theoretical perspective.

Table 3: Pure metal resistivity assumptions

Quasi free electrons  
 Photon-electron scattering  
 Fermi-Dirac distributions for electrons  
 Bose-Einstein distribution for phonons

Table 4: Residual resistivity assumptions

Quasi free electrons  
 Impurity-electron scattering  
 Fermi-Dirac distributions for electrons  
 Fixed scattering centers for impurities,  
 probable Fermi-Dirac distributions

Note that the dependence or independence of these two sets of assumptions is not at all clear in this case. There are a few dilute alloys that do not show the characteristics of Figure 6, e.g., gold in copper. This suggests it is not correct to assume that the NLAM-metric is a good representation of the measured resistivity.

To attempt to capture all of the characteristics that were observed, the following assumption was made, i.e., the two sets shown in Table 3 and 4 are not sufficiently independent. Applying Principle IV, a linear transformation will be used as an attempt to enhance the independence of the generating functions. In addition, it was assumed that a linear transformation, similar to the one given in Appendix A, will be used and that different angles will be introduced instead of a single angle to mix the two functions.

$$\rho_{Ti}^{\gamma/2} = \cos(\psi_T)\rho_T^{\gamma/2} + \sin(\psi_T)\rho_I^{\gamma/2} \quad (22)$$

$$\rho_{Ii}^{\gamma/2} = -\sin(\psi_I)\rho_T^{\gamma/2} + \cos(\psi_I)\rho_I^{\gamma/2} \quad (23)$$

$\rho_T$  and  $\rho_I$  are the generating functions given by Equations 17 and 18, and  $\rho_{Ti}$  and  $\rho_{Ii}$  are the generating functions that are assumed to exhibit a higher degree of independence. If the transformation is taken to be a quasi-rotation in the  $\{\rho_T, \rho_I\}$  space, i.e., a rotation that skews the axes, then a measurable difference should be obtained. If the angles  $\psi_T$  and  $\psi_I$  are equal, the NLAM-metric will be unaltered since it is invariant under rotation (Appendix A). Calculating the scalar product gives the NLAM-metric in terms of the original resistivity functions:

$$\rho^\gamma = \frac{1}{2}\rho_I^\gamma(2 + \cos(2\psi_I) - \cos(2\psi_T)) + \frac{1}{2}\rho_I^\gamma(2 - \cos(2\psi_I) + \cos(2\psi_T)) + \frac{1}{2}\rho_I^{\gamma/2}\rho_T^{\gamma/2}(-2\sin(2\psi_I) + 2\sin(2\psi_T)), \quad (24)$$

The DMR discrepancy function,  $\Delta/\rho_I$ , with this new NLAM-metric, Equation 24, is:

$$\frac{\Delta}{\rho_I} = \frac{\rho}{\rho_I} - \frac{(\rho_T + \rho_I)}{\rho_I} \quad (25)$$

With this transformed NLAM-metric, a richer variety of results can be obtained; in fact, all of the observed variations can be generated (Figure 7). With the proper choice of parameters, the deviation function, Equation 25, has the correct shape to account for the "hard to explain hump" that was observed in this system. Equation 25 also will generate all of observed shapes (depending on the physical parameters and the transformation angles), as illustrated in Fig. 7. The NLAM-metric has all of the characteristics observed in the experimental data. Basically, the shape of the deviation function,  $\Delta/\rho$ , depends on the values chosen for the impurity scattering resistivity and the transformation angles.

Making the assessment that the given generating functions were not independent and then applying a linear transformation, at least in this case, produced results that better represented the observed data, and it illustrates Principle IV. It is not necessary to go beyond this point, since the only purpose was to demonstrate that the observed deviations can be accounted for by the application of the NLAM-metric with  $\gamma \neq 1$ .

Of course this is a more subtle example because Mattheissen's Rule is actually an application of the metric with  $\gamma = 1$ . The interesting feature of this example is the use of a transformation (a skewed rotation) to enhance the results, and, in fact by doing so, all of the observed features of DMR studies are provided. It seems clear that the NLAM-metric, as originally constructed, is not a correct representation of the measured resistivity as was assumed, but it becomes closer to the measured results after the transformation. The skewed rotation mixes the original generation functions just enough to enhance the quantitative representation of the observed data. This example suggests that independence of the generating function is important.

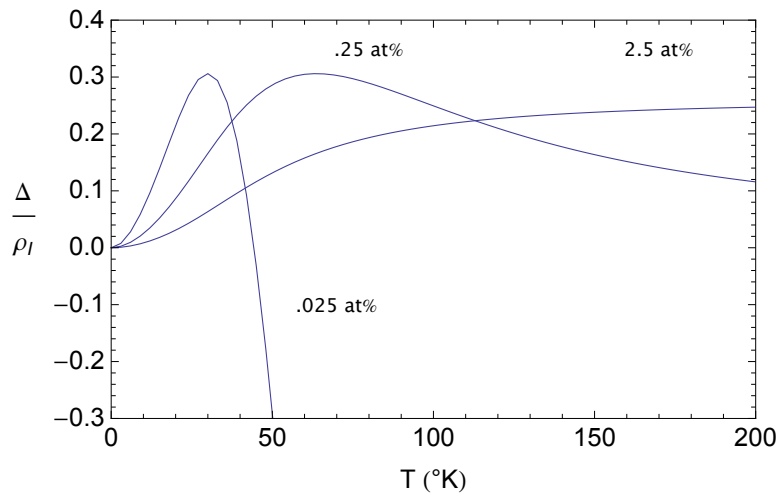


Figure 7: . All of the typical curves for Equation 25 vs. temperature can be generated after improving the independence of the two generating functions.

To show that it fits the data, take the measured results for 0.05 at% Au in Cu as an example (Dugdale and Basinski, [16]) as given in Bass ([10], Fig. 22). Obviously, a reasonable fit can be obtained (Figure 8).

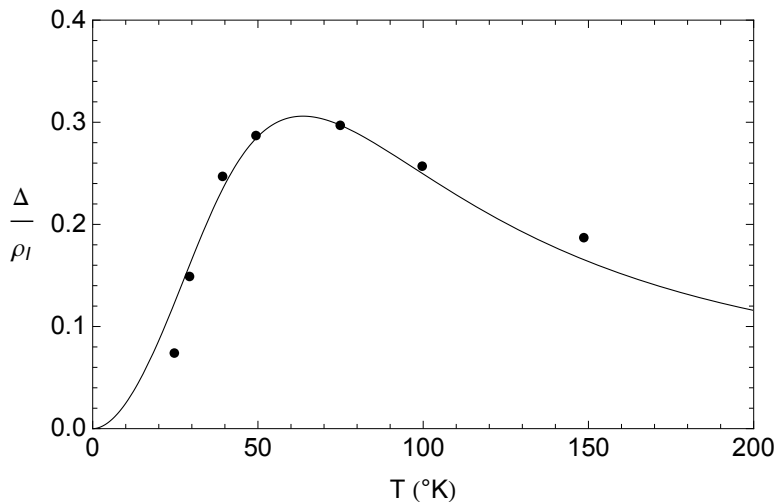


Figure 8: . Typical curve for Equation 25 vs. temperature for copper doped with gold showing the "hard to explain hump" (Bass [10])

## 6 EXAMPLE 4: WORK FUNCTION AS A FUNCTION OF SURFACE COVERAGE.

In this final example, the NLAM-metric is viewed from a more fundamental perspective as a means of deriving a complex theory from two very simple theoretical views. When the simple views are combined by the NLAM-metric, the result is an excellent representation of the experiments.

### 6.1 Background

This model for the surface work function first was used in a dispenser cathode life model, Longo [3]. The surface work function as a function of monolayer dipole coverage has received a great deal of attention for a good part of the last century. The basic understanding of the problem comes primarily from the work of Langmuir ([17- 19]). Many theories and models have been developed to describe these surface effects. Topping [20] developed a physical theory that has been used extensively. In recent times, Mueller [21, 22] used a cluster model expansion from quantum physics to determine the parameters of the Topping model as applied to dispenser cathodes. The results of the theory developed herein were compared with the results of Topping and Mueller. The work function developed by Topping and Mueller is given by:

$$\psi = \psi_0 + \Delta\psi \quad (26)$$

Where

$$\Delta\psi = \frac{-1.88\epsilon\mu_0 N}{1 + c\alpha N^{3/2}} \quad (27)$$

For details, see Topping-Mueller.

Two independent theories are required to apply the metric, each of which describes the surface as it accumulates dipoles. Let the parameter,  $\theta$ , be the fraction of the number of atoms added to the number of sites on the surface, this will be the independent parameter. Further, it will be assumed that atoms are added to the surface in a completely random way and that where they reside on the surface is independent of the previous history of the affected sites.

## 6.2 Theory 1

This theory describes the total non-contiguous area of a surface that remains uncovered as  $\theta$  increases, i.e., the fraction of sites on the substrate that remain free of Barium atoms. Let  $A_M$  be the sum of the non-contiguous area of the exposed substrate. With these definitions of  $A_M$  and  $\theta$ , the rate of change of the exposed substrate area as  $\theta$  changes will simply be proportional to the exposed area with a proportionality constant,  $\alpha$ :

$$\frac{dA_M(\theta)}{d\theta} = -\alpha A_M(\theta) \quad (28)$$

This generating theory simply describes the changes in the exposed number of substrate sites as the value of  $\theta$  changes. When  $\theta = 0$ , the exposed area, i.e.,  $A_M = A_G$ , is the geometric area of the surface. The solution is simply:

$$A_M(\theta) = A_G e^{-\alpha\theta} \quad (29)$$

This solution clearly applies and makes sense over the entire range of  $\theta$ . This theory presents a view, as seen by an outside observer, of the remaining area of the substrate that is unaffected by the addition of Barium atoms.

## 6.3 Theory 2

In theory 2, the surface is viewed as a barium surface the area of which increases as  $\theta$  increases. In this extreme, where  $\theta$  is large, a thick layer of barium atoms is built. An outside observer would see the area of the barium surface was increasing. Also, and perhaps more important, electrons that pass through sites that are two or more barium atoms thick will be influenced by the barium

atoms alone, and not be influenced by the underlying substrate.

Let  $A_{Ba}$  be the total non-contiguous area covered by multiple layers. In this calculation,  $\theta$  measures the sites that are covered by multiple barium atoms and not exposed to substrate sites. In this way, the covered sites are counted as having changed, but the definition of the sites remains the same. This shift in counting does not alter the definition of  $\theta$ ; it only alters the point of view of the observer. In a sense, this is analogous to the shift in the point of view of the basic emission theories discussed in example 1, only, this time, the same observation is counted in two different ways. As before the rate of change of the area  $A_{Ba}$  as  $\theta$  changes is proportional to the extent of the area covered. In general, the proportionality constant,  $\beta$ , will be different from the one used in the first theory. The differential equation is:

$$\frac{dA_{Ba}(\theta)}{d\theta} = -\beta A_{Ba}(\theta) \quad (30)$$

When  $\theta = 0$ , the area of the multiple layer is zero, i.e.,  $A_{Ba} = 0$ . And when  $\theta \rightarrow \infty$ , the multiple layer area,  $A_{Ba} = A_G$ , is the geometric area of the surface. What has changed is the boundary conditions. The solution is simply:

$$A_{Ba}(\theta) = A_G(1 - e^{-\beta\theta}) \quad (31)$$

and again it makes sense and applies over the entire range of  $\theta$ . Again, it is not a complete physical description of the surface; rather, it is the observer's count of multiple covered sites.

## 6.4 NLAM-metric description of the surface coverage

A complete physical description of the surface can be obtained by the application of the NLAM-metric using the two independent measures of the surface. The resulting area will be interpreted as the transition area, i.e., the area wherein the electrons that are passing through will experience the influence of the interaction between the substrate and the thick Barium layer. This is given by:

$$A(\theta) = (A_M^\gamma + A_{Ba}^\gamma)^{1/\gamma} \quad (32)$$

It is difficult to compare this with measured results because a non-contiguous surface coverage area is difficult, if not impossible, to measure on an atomic scale, but we can easily turn this into a work function that can be readily evaluated.

## 6.5 NLAM-metric description of the work-function

The work function over the entire range of  $\theta$  can be obtained by the following arguments. The generating functions for the work function are 1) the contribution to the work-function from the basic substrate, i.e., just a count of electrons

passing through sites that are unoccupied, i.e., proportional to the amount of the substrate that is exposed:

$$\phi_M(\theta) = \frac{A_M(\theta)}{A_G} \varphi_M. \quad (33)$$

2) the contribution to the work-function from the thick multilayer, which is just the count of the electrons that are passing through sites that are covered by more than one Barium atom:

$$\phi_{Ba}(\theta) = \frac{A_{Ba}(\theta)}{A_G} \varphi_{Ba}. \quad (34)$$

where  $\varphi_M$  is the work function of the bare substrate, e.g., for tungsten  $\varphi_M = 4.5eV$  and for barium  $\varphi_{Ba}$ , which is the work function of a thick barium surface, i.e., the work function if the substrate were pure barium,  $\varphi_{Ba} = 2.55eV$ .

The work-function through the transition is obtained by constructing an NLAM-metric with these two generating functions, i.e., Equations 33 and 34 combined with Equations 29 and 31, which gives:

$$\phi(\theta) = (\phi_M(\theta)^\gamma + \phi_{Ba}(\theta)^\gamma)^{1/\gamma} \quad (35)$$

This time, we find that when  $\gamma$  is positive,  $\phi(\theta)$  is a reasonable representation of the observed work function of the system. The precise shape of the result will depend on the choice of the proportionality constants,  $\alpha$  and  $\beta$ , and shape factor parameter,  $\gamma$ . The work-function as a function of the surface coverage,  $\theta$ , can be written as:

$$\phi(\theta) = \left( \left( \frac{\Gamma \varphi_M}{\varphi_{Ba}} \right)^{\frac{\Gamma \theta}{1-\Gamma}} \varphi_M \right)^\gamma + \left( \varphi_{Ba} \left( 1 - \left( \frac{\Gamma \varphi_M}{\varphi_{Ba}} \right)^{\frac{\theta}{1-\Gamma}} \right) \right)^\gamma \right)^{1/\gamma} \quad (36)$$

where  $\Gamma = \alpha/\beta$ , and is obtained by differentiating equation 36 and setting it to zero, where the work-function is a minimum. That this is a reasonable representation of the effect of work function on surface coverage can be seen in Figure 9, which compares Equation 36 with the Mueller-Topping calculation for a particular type of cathode called an M-type dispenser cathode.<sup>3</sup>, an osmium emitter surface  $\varphi_M = 4.7eV$  with barium surface atoms. The parameters for the fit are  $\Gamma = 2.702$  and  $\gamma = 1.18$

---

<sup>3</sup>An M-type dispenser cathode is a tungsten dispenser cathode with an osmium alloy deposited on the surface.

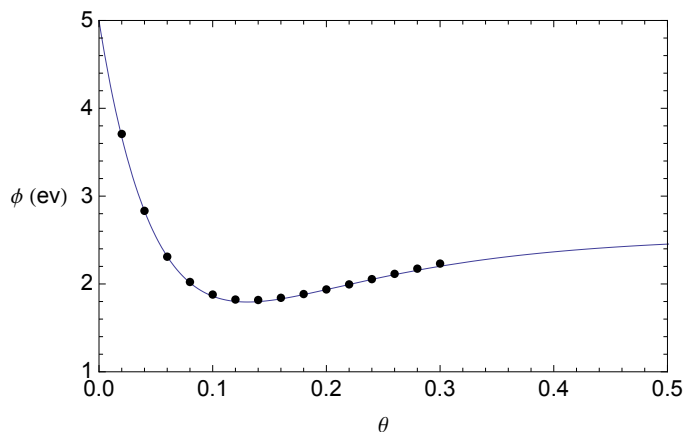


Figure 9: Work Function vs surface coverage  $\theta$ , The data points are from Mueller-Topping.

Actually, over a broader range, the metric provides a representation that is physically more satisfactory since it approaches the value of the work function of the thick barium level, whereas the Mueller-Topping model continues to climb to higher values, as seen in Figure 10. The comparison is made over a wide range of dipole coverage even though the depolarization model (i.e., the Mueller-Topping model) is really only valid up to the minimum.)

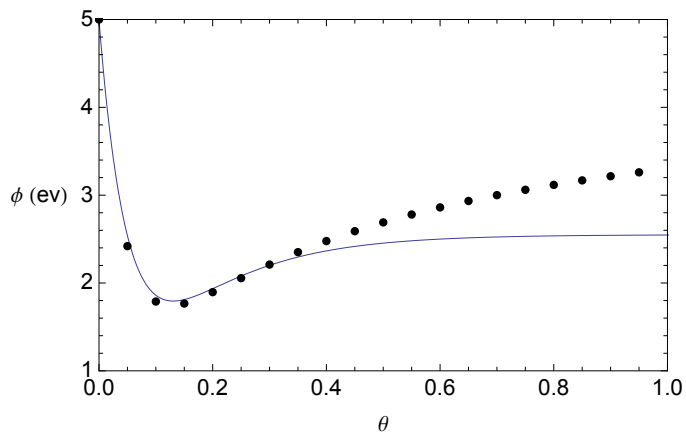


Figure 10: Work Function vs surface coverage over longer range of  $\theta$

In this example a complex system was modeled theoretically using principles I, III, and V to develop the two asymptotic theories from simple counting concepts envisioned from two distinct and independent points of view from the same data. The results were excellent; the maximum discrepancy between this model

and an existing theoretical model was  $\pm 0.008eV$ , from  $\theta = 0$  to a small distance beyond the minimum, and this discrepancy probably is below the measurement detectability level. This example further demonstrates that the final result was constrained by the asymptotic nature of the generating functions, whereas the very thick limit of the Mueller-Topping model is not consistent with the expectations of a barium surface, as the generating function suggests.

## 7 THE $\gamma$ FACTOR CONTAINS FUNDAMENTAL PHYSICS

Even though the unit-less numerical parameter,  $\gamma$ , was introduced to build an engineering model for the thermionic emission process,  $\gamma$  contained some deeper physics. To understand the physical property of the numerical parameter, it is necessary to understand the paradigm of workers in the field of thermionic emissions, with regards to the shape of the emission curve. The theory indicated that it should have a sharp transition between the space charge and the temperature limit, whereas it always has a more rounded transition. There have been several studies that were directed at theoretically predicting the shape (Scott [23], Tonnerre [24]). It became a consensus that the behavior was due to the non-uniformity of the surface of the emitter due to patches of high and low work-function regions. However, this was shown to be unsupportable (Adler [25]). From a detail theoretical study of Equation 7, as compared to a statistical mechanics theory of surfaces, a direct relationship was found between  $\gamma$  and the surface entropy of the emitter (Longo [26]). Thus, the shape of the emission curve was due to non-uniform emissions, but not as originally envisioned; rather it was the direct result of thermodynamics. Life tests of the emitter clearly showed that the work function increased with time as did the surface entropy.

## 8 CONCLUSIONS

A general, nonlinear asymptotic principle was introduced for modeling complex systems, which we called NLAM-metric in that it was a measure of some physical property of a system. This technique was first envisioned from an engineering perspective, and its success suggests a more general principle may be involved. The NLAM-metric was constructed from physical theories that were derived independently from distinct perspectives and when combined using the NLAM-metric can result in a very good representation of more complex systems. More importantly, it does not require making physical measurements in regions where the pertinent physical theories strictly apply, but it constrains the interpretation of the measurements to be asymptotically consistent with the physical theories.

The NLAM technique was stated as a set of principles and was illustrated by means of four examples. In the cases that were illustrated, the fidelity of the theoretically-modeled representation and the experimental measurements were very good over the entire range of the independent variables defined by the asymptotic physical theories. The NLAM technique was demonstrated on a range of non-related physical systems to show that it appears not to be a coincidence of one special problem and also to lend credence to the generalization of the technique.

The NLAM-metric, Equation 7, was developed from an engineering perspective and was applied for more than 20 years with considerable usefulness and success in dealing with thermionic emissions. The use of Equation 7 was directly responsible for understanding the basic mechanisms that control the lifecycle of thermionic dispenser cathodes that are used in high power TWT, enhancing their expected useful life from 2 to 5 years to 25 to 30 years. The order of magnitude increase in life expectancy made higher power space communication economically practical.

By assuming Equation 7 to be a true physical representation of the emission process, it was shown that the parameter,  $\alpha$ , was derived from statistical mechanics and is the entropy of the emitter surface (Longo [26]). This correlates with the long-held belief that the lack of a sharp transition in emission was related to the non-uniformity of the surface, but, instead of small patches at different work functions, as was believed, the non-uniformity is a thermodynamic effect.

As a final comment, there may be insight into the NLAM-metric that is more fundamental. In the resistivity example, the results suggested that the independence of the generating function was important rather than just a curiosity. In the last example, something even more unexpected was suggested. How an observer looks at the problem makes an important difference. There is strong evidence in quantum mechanics, in particular the double-slit experiment, that the consciousness of an observer can alter the results of the experiment (Radin [27]). The result of the last example suggests that this might also be true in the classical realm, since the only difference between the two generating functions was how the observer decided to interpret counts, thus producing two independent theories with exactly the same data. Longo [28] provides thoughts concerning how real physical observers interact with the physical world.

## 9 APPENDIX A. ROTATIONAL INVARIANCE

If the independent variable are taken to be  $X_1^{\gamma/2}$  and  $X_2^{\gamma/2}$ , instead of  $X_1$  and  $X_2$ , then a linear coordinate transformation can be written,

$$Y_1^{\gamma/2} = a_{11}X_1^{\gamma/2} + a_{12}X_2^{\gamma/2} \quad (37)$$

$$Y_2^{\gamma/2} = a_{21}X_1^{\gamma/2} + a_{22}X_2^{\gamma/2} \quad (38)$$

Now if we assume that the transformation is a simple rotation in the  $X_1, X_2$  space the matrix becomes

$$\begin{pmatrix} a_{11} & a_{12} \\ a_{21} & a_{22} \end{pmatrix} = \begin{pmatrix} \cos(\theta) & \sin(\theta) \\ -\sin(\theta) & \cos(\theta) \end{pmatrix} \quad (39)$$

The two equations above can be written

$$\begin{pmatrix} Y_1^{\gamma/2} \\ Y_2^{\gamma/2} \end{pmatrix} = \begin{pmatrix} \cos(\theta) & \sin(\theta) \\ -\sin(\theta) & \cos(\theta) \end{pmatrix} \begin{pmatrix} X_1^{\gamma/2} \\ X_2^{\gamma/2} \end{pmatrix} \quad (40)$$

Taking the scalar product of this result we get the metric

$$Z^\gamma = Y_1^\gamma + Y_2^\gamma = X_1^\gamma + X_2^\gamma \quad (41)$$

which demonstrates rotational invariance.

## 10 REFERENCES

1. R.T. Longo, IEDM Technical Digest, 152, (1978)
2. R.T. Longo, IEDM Technical Digest, 467, (1980)
3. R.T.Longo, E.A. Adler, L.R.False, IEDM Technical Digest, 318, (1984)
4. O.W. Richardson, Emission of Electricity from Hot Bodies, (1921)
- 5 S. Dushman, I.W. Ewald, Physic. Rev. 29, 857, (1927)
6. W. Schottky, Physik Z.15, 526, (1914).
7. Child, Phys. Rev., 32, 492, (1911)
8. I. Langmuir, Phys. Rev., 17, 441, (1921)
9. A.Matthiessen, Annalen der Physik und Chemie, p190, (1860); A.Matthiessen, Annalen der Physik und Chemie, p19, (1864)
10. J. Bass, Advances in Physics, Vol 21. Issue 91, 431,(1972)
11. W.Shockley,Electrons and Holes in semiconductors,D.Van Nostrand Comp,Inc.(1950)
- 12 A.S.Gilmour,Jr. Klystrons,Traveling Wave Tubes, Magnetrons,Crossed-Field Amplifiers, ans Gyrotrons, Artech House, (2011)
13. R.Vaughan,IEEE Trans.Elect.Devices, 33, 11, (1986)
14. American Institute of Physics Handbook,McGraw Hill, (1957)
15. J.Bardeen, Journal of Applied Physics, Vol 11, 88,(1940)
- 16 Dugdale and Basinski; see Bass, reference 3.
- 17 I. Langmuir, J. Am. Chem. Soc., 54 2798, (1932)
- 18 I. Langmuir, Chem. Revs. ,13, 147, (1933)
- 19 I. Langmuir, J. Chem. Soc., 511, (1940)
- 20 J. Topping, Proc. Roy. Soc., (London) A114, 67, (1927)
- 21 W.Mueller,IEEE Trans.Elect.Dev.36,180,(1989))
- 22 W.Mueller, IEDM Technical Digest, 339, (1991)
- 23 J. B. Scott, J. Appl. Phys. 52, 4406 (1981)

- 24 J. C. Tonnere, D. Brion, P. Palluel, and A. M. Shroff, *Appl. Surf. Sci.* 16, 238 (1983)
25. E.A. Adler, R.T.Longo, *Journal of Applied Physics*, 59,1022 (1986)
26. R.T.Longo, *Journal of Applied Physics*, 94, 6966, (2003)
- 27 Radin D et al. , 2012. Consciousness and the double-slit interference pattern: Six experiments. *Physics Essays*. [http:// deanradin. com/ evi- dence/ Radin2012doubleslit. pdf](http://deanradin.com/evidence/Radin2012doubleslit.pdf) , 25(2)
- 28 R,T,Longo 2014, viXra:1405.0244